

Andreev Bound States Formation and Quasiparticle Trapping in Quench Dynamics Revealed by Time-Dependent Counting Statistics

R. Seoane Souto, A. Martín-Rodero, and A. Levy Yeyati

Departamento de Física Teórica de la Materia Condensada, Condensed Matter Physics Center (IFIMAC) and Instituto Nicolás Cabrera, Universidad Autónoma de Madrid, E-28049 Madrid, Spain

(Received 24 June 2016; published 21 December 2016)

We analyze the quantum quench dynamics in the formation of a phase-biased superconducting nanojunction. We find that in the absence of an external relaxation mechanism and for very general conditions the system gets trapped in a metastable state, corresponding to a nonequilibrium population of the Andreev bound states. The use of the time-dependent full counting statistics analysis allows us to extract information on the asymptotic population of even and odd many-body states, demonstrating that a *universal* behavior, dependent only on the Andreev state energy, is reached in the quantum point contact limit. These results shed light on recent experimental observations on quasiparticle trapping in superconducting atomic contacts.

DOI: 10.1103/PhysRevLett.117.267701

Superconducting nanodevices are of central interest as building blocks of future quantum information processors. While traditionally based on Josephson junction architectures [1], superconducting quantum dots and quantum point contacts are now being explored for quantum information applications like the generation of electron entanglement through Cooper pair splitting [2,3] and the so-called Andreev qubits [4]. Similar hybrid systems can host Majorana-like excitations whose search and potential applications are generating huge research activity in the condensed matter community [5]. Within this context, studies of the transient response of superconducting nanodevices are of basic as well as practical interest [6]. This is connected with the unexplained evidence of residual non-equilibrium quasiparticles which undermines the quantum coherence in these devices [7]. In the case of superconducting atomic contacts (SACs), this phenomenon manifests in the presence of long-lived trapped quasiparticle states within their Andreev bound states (ABSs) [8,9].

In the present work, we address these questions by analyzing the quench dynamics in the formation of a phase-biased superconducting single-channel contact. We consider the situation schematically depicted in Fig. 1, where a central electronic level is abruptly coupled to two superconducting leads [Fig. 1(a)]. Our main question concerns the properties of the state which is generated at intermediate times (i.e., $\tau_{\text{in}} \gg t \gg \hbar/\Delta$, where τ_{in} is a characteristic inelastic relaxation time and Δ is the superconducting gap). We find that for generic values of the parameters the system gets trapped into a *metastable* state, reflecting a nonequilibrium population of the ABSs and exhibiting a smaller or even opposite supercurrent to the one expected for thermal equilibrium. While for weak coupling to the leads $\Gamma < \Delta$ this state depends strongly on the initial conditions, at large Γ it reaches a “universal” behavior

dependent only on the Andreev level position within the gap but still deviating from the equilibrium population. Furthermore, we study the transient process in terms of charge transfer probabilities derived from the time-dependent full counting statistics (FCS) analysis. This allows us to determine the separate populations of even and odd parity states, information which is inaccessible from any mean field study of single-particle properties. We find that the odd parity states, corresponding to the trapping of a quasiparticle within the ABSs, get a significant population $\sim 0.2\text{--}0.5$ for a broad range of parameters, in agreement with the experimental observations for SACs [4,8].

Model and formalism.—Our model nanojunction is composed of three regions: a central spin-degenerate electron level (which can be initially empty or occupied) and two BCS superconducting leads. These are connected at $t = 0$ by a tunnel Hamiltonian $H_T(t)$, creating excited quasiparticles which undergo multiple tunneling events between the electrodes. In particular, successive Andreev

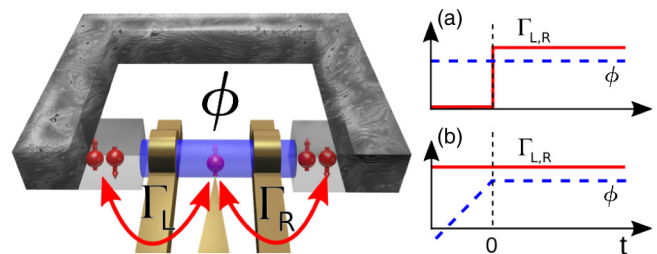


FIG. 1. Schematic representation of the nanojunction formation process considered in this work. In case (a) the tunneling amplitudes between the central region and the leads are suddenly connected at $t = 0$, while in case (b) the tunnel amplitudes are constant but there is a bias voltage switch off at $t = 0$. The nanojunction is formed on a superconducting loop threaded by a magnetic field which allows us to fix the phase difference ϕ .

reflections are needed to develop the ABSs within the gap at energies $\pm\epsilon_A$ and to establish a nondissipative (Josephson) current through the device. The system Hamiltonian $H = H_{\text{leads}} + H_0 + H_T$ can be written in terms of Nambu spinors $\hat{\Psi}_j^\dagger = (c_{j\uparrow}^\dagger, c_{j\downarrow})$, where $j = k\nu, 0$ denotes the $\nu = L, R$ lead and the central level, respectively. We have $H_0 = \hat{\Psi}_0^\dagger \hat{h}_0 \hat{\Psi}_0$, $H_{\text{leads}} = \sum_{k\nu} \hat{\Psi}_{k\nu}^\dagger \hat{h}_{k\nu} \hat{\Psi}_{k\nu}$, and $H_T = \sum_{k,\nu} (\hat{\Psi}_{k\nu}^\dagger \hat{V}_\nu(t) \hat{\Psi}_0 + \text{H.c.})$, where $\hat{h}_0 = \epsilon_0 \sigma_z$ and $\hat{h}_{k\nu} = \epsilon_{k\nu} \sigma_z + \Delta_\nu \sigma_x$ (σ_z and σ_x denote here Pauli matrices in Nambu space). For describing an abrupt switch on into a phase-biased situation, we use $\hat{V}_\nu(t) = \theta(t) V_\nu^0 \sigma_z e^{i\sigma_z \phi_\nu}$, where $\phi_L - \phi_R = \phi$ determines the phase difference between the leads and $\theta(t)$ is the Heaviside function. While this initialization can be considered somewhat artificial, it generates the same dynamics as a large applied bias voltage which is suddenly switched off at $t = 0$ [see Fig. 1(b) and Supplemental Material [10]]. For simplicity, we consider a constant normal density of states $\rho_{L,R}$ in the leads with a finite bandwidth W taken as the larger energy scale in the model, and we define the stationary tunneling rates as $\Gamma_\nu = \pi (V_\nu^0)^2 \rho_\nu$, and $\Gamma = \Gamma_L + \Gamma_R$. The central level initial charge will be denoted by $n_\sigma(0)$, where $\sigma \equiv \uparrow, \downarrow$. Hereafter, we assume $\hbar = e = 1$.

The transport properties of the system are fully characterized by the generating function (GF) defined on the Keldysh contour as [13]

$$Z(\chi, t) = \left\langle T_K \exp \left(-i \int_C dt' H_{T,\chi}(t') \right) \right\rangle_0, \quad (1)$$

where $\chi \equiv \chi_\nu(t)$ are counting fields entering as phase factors modulating the hopping terms in H_T and having opposite values $\pm\chi_\nu$ on the two branches of the Keldysh contour. The average in Eq. (1) is taken over the decoupled system. The GF gives access to the charge transfer cumulants, i.e., $C_n(t) = (i^n \partial^n S / \partial \chi^n)_0$, where $S = \ln Z(\chi, t)$. For definiteness, we will hereafter assume $\chi_L = \chi$ and $\chi_R = 0$, thus focusing on charge transfer through the left interface. The corresponding current cumulants are given by $I^n(t) = \partial C_n / \partial t$. One can also decompose the GF as $Z(\chi, t) = \sum P_n(t) e^{i\chi n}$, where $P_n(t)$ can be associated with the probability of transferring n charges in the measuring time t . In the BCS superconducting case, the charge in the leads is not well defined, and $P_n(t)$ can eventually take negative values [14–16]. The $P_n(t)$ are therefore referred to as *quasiprobabilities*.

It can be shown that $Z(\chi, t)$ can be computed as a Fredholm determinant on the Keldysh contour [17–19]. A straightforward extension of this formalism to the superconducting case leads to

$$Z(\chi, t) = \det [\mathbf{G}(\chi = 0) \mathbf{G}(\chi)^{-1}], \quad (2)$$

where $\mathbf{G} = -i \langle T_K \Psi_0(t) \Psi_0^\dagger(t') \rangle$ is the Green function of the dot coupled to the leads defined in Keldysh-Nambu space.

For a generic situation, we evaluate Eq. (2) numerically following the approach described in Supplemental Material [10]. Analytical results allow us to further clarify our findings in certain limits as described below.

Current, charge, and spectral density evolution.—We first analyze the transient regime for these basic quantities. Results for the current evolution are shown in the upper panel in Fig. 2 for different values of the tunneling rates, phase difference $\phi/\pi = 0.64$, and for an initial condition $(n_\uparrow(0), n_\downarrow(0)) = (0, 1)$. We concentrate here in the highly transmitted, electron-hole symmetric case (i.e., $\epsilon_0 = 0$, $\Gamma_L \simeq \Gamma_R$) where the nonequilibrium effects that we discuss in this work are more pronounced. Moreover, when $\Gamma \gg \Delta$, this case corresponds to a highly transmitted single-channel SAC. In the electron-hole symmetric case, the stationary ABSs are roughly located at $\epsilon_A \simeq \tilde{\Delta} \sqrt{1 - \tau \sin^2(\phi/2)}$, where $\tau = 4\Gamma_L \Gamma_R / \Gamma^2$ is the normal transmission and $\tilde{\Delta} < \Delta$ varies from $\tilde{\Delta} \sim \Gamma$ for $\Gamma \ll \Delta$ to $\tilde{\Delta} \rightarrow \Delta$ for $\Gamma \gg \Delta$ [21]. As can be observed, the current reaches an asymptotic value smaller than the thermal equilibrium stationary one (indicated by the arrows in Fig. 2), becoming even of opposite sign in the case of $\Gamma \lesssim \Delta$.

Further insight on this behavior can be obtained by analyzing the evolution of the central region occupied spectral density (the method used to extract this quantity is described in Supplemental Material [10]). The lower panels in Fig. 2 clearly illustrate the process of formation of the

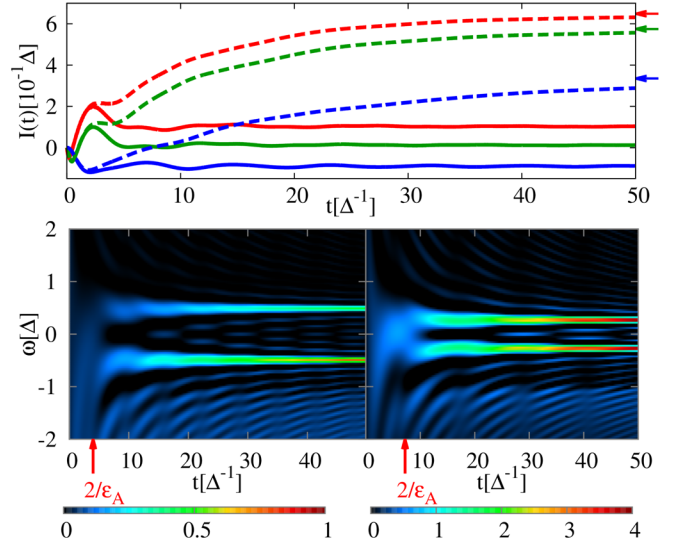


FIG. 2. The upper panel shows the transient current for different Γ/Δ values (from top to bottom: 10, 5, and 1) and a fixed phase difference $\phi/\pi = 0.64$ for the perfect transmission case. The solid lines correspond to the case of no external relaxation mechanism, and the dashed ones correspond to adding a phenomenological broadening in the spectral densities of size $1/\tau_{\text{in}} = 0.02\Delta$ [20]. The arrows indicate the stationary values for thermal equilibrium. The lower panels show the corresponding time-dependent occupied spectral densities for $\Gamma/\Delta = 10$ (left) and $\Gamma/\Delta = 1$ (right).

subgap states, whose spectral weight mainly originates from the lower continuous spectrum at $\omega < -\Delta$. In addition, the continuous spectrum exhibits oscillations which are gradually damped. As can be observed, it requires a characteristic time $\sim 2/|\epsilon_A|$ for the ABSs to become well defined [22]. The plots also show that while for $\Gamma \gg \Delta$ the lower ABS becomes more populated, there is an inversion in their population for $\Gamma \lesssim \Delta$.

Low tunneling rate regime.—In this regime, the contribution from the continuum states to the level charge becomes negligible. As described in Supplemental Material [10], this allows us to obtain an analytical expression for the population of the ABSs in this limit. Assuming the initial condition $(n_\uparrow, n_\downarrow) = (0, 1)$, these are given by

$$n_\pm(t) = \frac{\Gamma}{\pi} \int_{-W}^{-\Delta} \frac{(\omega \mp \Delta \cdot \epsilon_A/\Gamma)[\cos(\omega_\pm t) - 1]}{\omega_\pm^2 \sqrt{\omega^2 - \Delta^2}} d\omega, \quad (3)$$

where $+$ ($-$) corresponds to the upper (lower) ABS and $\omega_\pm = \omega \mp \epsilon_A$. As shown in the upper panel in Fig. 3, the comparison of $n_+ + n_-$ with the total spin-up charge obtained numerically for $\Gamma = 0.05\Delta$ yields very good

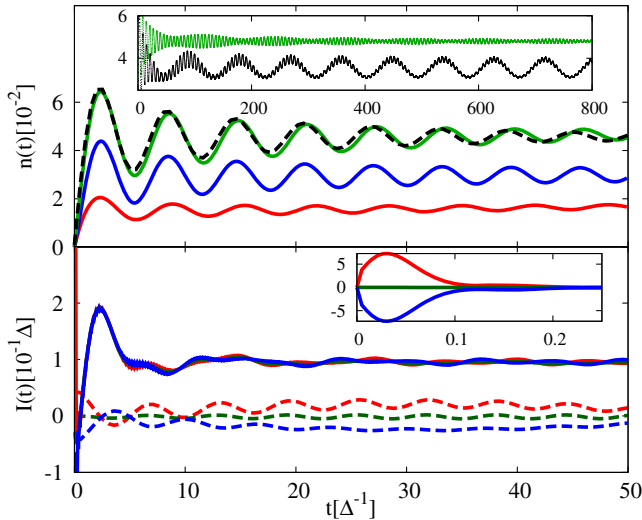


FIG. 3. The upper panel shows the ABS populations n_+ (blue line) and n_- (red line) for the case of the initial condition $(n_\uparrow, n_\downarrow) = (0, 1)$ with $\Gamma = 0.05\Delta$ and $\phi/\pi = 0.64$ as determined from Eq. (3). The dashed line corresponds to the total spin-up charge obtained numerically, and the green line corresponds to $n_+ + n_-$. The inset in the upper panel illustrates the evolution of the level charge on a larger time scale in an electron-hole symmetric ($\epsilon_0 = 0$, green curve) and nonsymmetric situation ($\epsilon_0 = 0.025\Gamma$, black curve). The black curve has been shifted down for clarity. The lower panel illustrates the dependence of the transient current on the initial condition for the perfect transmission case with $\Gamma/\Delta = 10$ (solid lines) and $\Gamma/\Delta = 0.05$ (dashed lines). The three initial conditions considered were $(n_\uparrow, n_\downarrow) = (0, 0)$ (red lines), $(0, 1)$ (green lines), and $(1, 1)$ (blue lines). The inset corresponds to an enlargement at very short times for the large Γ case.

agreement. Both n_+ and n_- exhibit an initial linear increase [23], with a slope set by Γ , followed by an oscillatory behavior with a characteristic period set by $\sim 2\pi/(\Delta \pm \epsilon_A)$. For $\Gamma \ll \Delta$ and $t > 1/\Delta$, $n_\pm(t)$ is well described by the expression

$$n_\pm(t) = n_\pm(\infty) + \frac{\Gamma}{\Delta} \left(1 \pm \frac{\epsilon_A}{\Gamma}\right) \frac{\sin[(\Delta \pm \epsilon_A)t - \frac{\pi}{4}]}{\sqrt{2\pi\Delta \cdot t}}, \quad (4)$$

where $n_\pm(\infty) = (\Gamma/2 \pm \epsilon_A/\pi)/\Delta$. This expression indicates that the oscillatory behavior dies out with a weak power law (i.e., as $t^{-1/2}$). While in this limit the upper level is more populated than the lower one, Eq. (3) would predict an inversion of the relative populations for $\Gamma/\Delta \sim 1$. Although for $\Gamma \gtrsim \Delta$ the contribution from the continuum to the system dynamics can no longer be neglected, the prediction of the population inversion is consistent with the numerical results for the current shown in the upper panel in Fig. 2.

It is important to notice that when electron-hole symmetry is broken ($\epsilon_0 \neq 0$) the switch-on process couples the two ABSs, thus generating an additional contribution to the level charge which oscillates with a frequency $2\epsilon_A$ (see the inset in the upper panel in Fig. 3). A more detailed analysis of this case is provided in Supplemental Material [10].

Dependence on initial conditions.—The fact that the system reaches a metastable state suggests that this can be extremely sensitive to the initial conditions. This is true for the low Γ regime, but this sensitivity gradually disappears for increasing Γ . This is illustrated in the lower panel in Fig. 3, where the current in the perfect transmission case for $\Gamma = 0.05\Delta$ and $\Gamma = 10\Delta$ is shown for three different initial conditions $(n_\uparrow, n_\downarrow) = (0, 0)$, $(0, 1)$, $(1, 1)$. It is observed that a positive or negative peak in I of size $\sim \Gamma_L$ appears at short times when the initial charge deviates from the expected stationary value. This peak, however, relaxes in a time scale set by $1/\Gamma$, as illustrated in the inset in the lower panel in Fig. 3.

FCS analysis.—New light on the system dynamics can be shed by analyzing the quasiprobabilities $P_n(t)$. We first focus in the large Γ/Δ limit where, as commented before, the influence of the initial conditions is less pronounced. A clear picture emerges when $P_n(t)$ is analyzed as a function of n as in Fig. 4, where a density plot of $P_n(t)$ on the (t, n) plane is shown. One can clearly identify here three main lines with slopes I_- , I_{odd} , and I_+ , which can be associated with three different coexisting many-body states. The character of these states can be inferred from the slope values. Thus, $I_- \sim 2\partial\epsilon_A/\partial\phi$ corresponds to the system ground state, $I_+ \sim -I_-$ can be associated with the even excited state, and $I_{\text{odd}} \sim 0$ would correspond to an odd state with a trapped quasiparticle within the ABSs (this last state is spin degenerate) [8]. A slight deviation of the slopes from these values arises from the contribution of the continuum

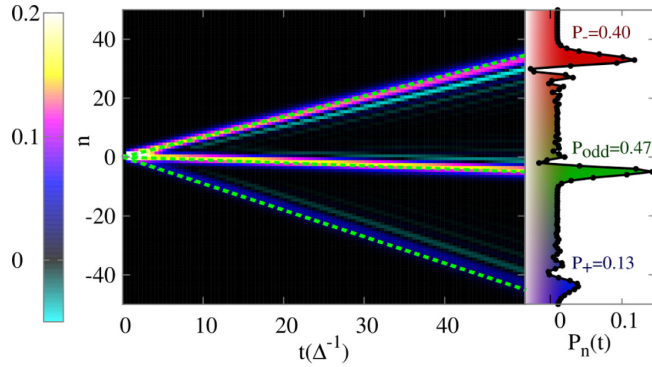


FIG. 4. Density plot of $P_n(t)$ in the (t, n) plane for the perfect transmission case with $\Gamma/\Delta = 10$ and $\phi/\pi = 0.64$. The dashed lines are slopes corresponding to the current in the different coexisting many-body states (see the text). The right inset shows a cut of $P_n(t)$ at $t = 50\Delta^{-1}$, demonstrating that three asymptotic populations can be clearly identified.

to the supercurrent which becomes negligible in the $\Gamma/\Delta \rightarrow \infty$ limit.

We can further characterize the metastable state by the weights P_- , P_+ , and P_{odd} of these three many-body states. An interesting feature of the system evolution is that once the ABSs become well defined (at times of the order of $2/|\epsilon_A|$) these weights remain nearly constant as far as no external relaxation mechanism is operative on this time scale. In order to extract these weights, two procedures can be used: (i) directly from the $P_n(t)$ at sufficiently large times, integrating the P_n around the three peaks (see the right inset in Fig. 4) and (ii) using the mean current, the mean noise, and the normalization condition to set a system of three equations with three unknowns from which P_+ , P_- , and P_{odd} can be extracted (see Supplemental Material [10]). Both procedures yield results which are in good agreement. Figure 5 shows the resulting asymptotic weights as a function of ϵ_A for two different values of Γ/Δ . In the case $\Gamma/\Delta = 10$ (left panel), the odd state exhibits an increasing population with decreasing ϵ_A reaching a value of the order of 0.5 when $\epsilon_A \rightarrow 0$. At the same time, P_{\pm} tend to converge to the value 0.25 in this limit. As in the case of the current, the results for this large Γ case are rather insensitive to the particular choice of the initial conditions. Moreover, the results in this limit are *universal* depending only on ϵ_A irrespective of the junction transmission, as shown by squares ($\tau = 0.95$) and circles ($\tau = 0.9$) in the left panel in Fig. 5. These results are in remarkable agreement with those of Ref. [4], which were obtained for a SAC with $\tau \sim 0.99$ and could be qualitatively understood in terms of a simple rate equation picture where the even ground state, the two odd states, and the excited even state are connected by some effective rates, as depicted in the inset in Fig. 5. Within this simplified picture and taking $\Gamma_{\text{odd}} \sim 1/\Delta$ and $\Gamma_{\pm} \sim 1/(\Delta \pm \epsilon_A)$, i.e., inversely proportional to the energy distance between the

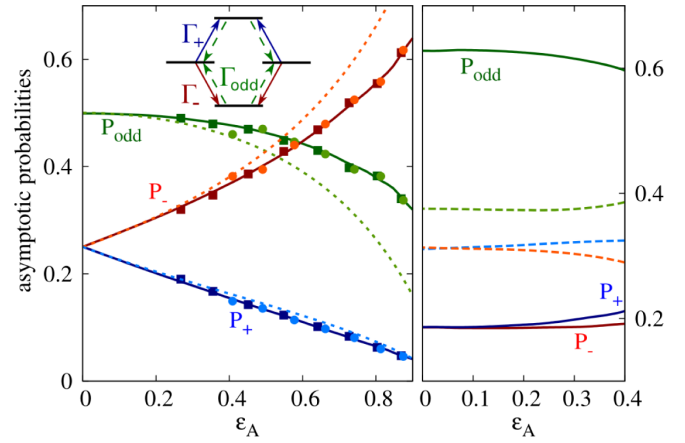


FIG. 5. The left panel shows the asymptotic probabilities P_{\pm} and P_{odd} for $\Gamma/\Delta = 10$ as a function of the ABS energy ϵ_A . Solid lines correspond to perfect transmission, squares to $\tau = 0.95$, and dots to $\tau = 0.9$. The dashed lines are results obtained with the simple rate equation model schematically depicted in the inset and assuming $\Gamma_{\text{odd}} \sim 1/\Delta$ and $\Gamma_{\pm} \sim 1/(\Delta \pm \epsilon_A)$. The right panel corresponds to $\Gamma/\Delta = 1$, perfect transmission, and two different initial conditions $(n_{\uparrow}, n_{\downarrow}) = (0, 1)$ (solid lines) and $(0, 0)$ (dashed lines).

states and the continuum, one obtains the results indicated by the dashed lines in the left panel in Fig. 5, which are in good agreement with the numerical ones (see [10] for more details). In contrast, the results become increasingly sensitive to the initial conditions for decreasing Γ/Δ . As shown in the right panel in Fig. 5, for $\Gamma/\Delta = 1$ the asymptotic populations for different initial conditions strongly deviate from each other.

One should finally comment on the effect of additional relaxation mechanisms. In Ref. [9], the relaxation through photon and phonon emission was analyzed using a rate equation approach, obtaining a semiquantitative agreement with the experimental results of Ref. [8] in the stationary regime. This approach, however, is not able to describe the initial stages of the ABS formation which can be addressed by the present microscopic theory. In fact, one can identify P_{odd} with the “initial poisoning” probability defined in Ref. [8]. A direct experimental test of the universal behavior predicted for this quantity would require analyzing the response to large voltage pulses.

Conclusions.—We have shown that the transient dynamics in the formation of a phase-biased superconducting nanojunction leads to a metastable state characterized by a nonequilibrium population of the system ABSs. Although in the quantum dot regime this state is strongly sensitive to the initial conditions, in the quantum point contact limit this sensitivity disappears and a universal asymptotic population is reached, dependent only on the ABS energy levels. These findings shed light on the available experimental results like those of Refs. [4,8] and could be tested more thoroughly in future experiments.

We acknowledge discussions with R. Avriller, C. Urbina, and L. Arrachea and financial support by Spanish MINECO through Grant No. FIS2014-55486-P and the “María de Maeztu” Programme for Units of Excellence in R&D (MDM-2014-0377). Computer resources by the Supercomputing and Visualization Center of Madrid (CeSViMa) and the Spanish Supercomputing Network (RES) are also acknowledged.

-
- [1] M. H. Devoret and R. J. Schoelkopf, *Science* **339**, 1169 (2013).
- [2] L. Hofstetter, S. Csonka, J. Nygård, and C. Schönenberger, *Nature (London)* **461**, 960 (2009).
- [3] L. G. Herrmann, F. Portier, P. Roche, A. L. Yeyati, T. Kontos, and C. Strunk, *Phys. Rev. Lett.* **104**, 026801 (2010).
- [4] C. Janvier, L. Tosi, L. Bretheau, Ç. Ö. Girit, M. Stern, P. Bertet, P. Joyez, D. Vion, D. Esteve, M. F. Goffman, H. Pothier, and C. Urbina, *Science* **349**, 1199 (2015).
- [5] For reviews, see J. Alicea, *Rep. Prog. Phys.* **75**, 076501 (2012); C. W. J. Beenakker, *Rev. Mod. Phys.* **87**, 1037 (2015).
- [6] Some previous works have addressed time-resolved Josephson transport in superconducting nanojunctions; see, for instance, E. Perfetto, G. Stefanucci, and M. Cini, *Phys. Rev. B* **80**, 205408 (2009); G. Stefanucci, E. Perfetto, and M. Cini, *Phys. Rev. B* **81**, 115446 (2010); B. Tarasinski, D. Chevallier, J. A. Hutasoit, B. Baxevanis, and C. W. J. Beenakker, *Phys. Rev. B* **92**, 144306 (2015); J. Weston and X. Waintal, *Phys. Rev. B* **93**, 134506 (2016).
- [7] J. M. Martinis, M. Ansmann, and J. Aumentado, *Phys. Rev. Lett.* **103**, 097002 (2009); G. Catelani, R. J. Schoelkopf, M. H. Devoret, and L. I. Glazman, *Phys. Rev. B* **84**, 064517 (2011); D. Ristè, C. C. Bultink, M. J. Tiggelman, R. N. Schouten, K. W. Lehnert, and L. DiCarlo, *Nat. Commun.* **4**, 1913 (2013); E. M. Levenson-Falk, F. Kos, R. Vijay, L. Glazman, and I. Siddiqi, *Phys. Rev. Lett.* **112**, 047002 (2014).
- [8] M. Zgirski, L. Bretheau, Q. Le Masne, H. Pothier, D. Esteve, and C. Urbina, *Phys. Rev. Lett.* **106**, 257003 (2011).
- [9] D. G. Olivares, A. L. Yeyati, L. Bretheau, C. O. Girit, H. Pothier, and C. Urbina, *Phys. Rev. B* **89**, 104504 (2014); A. Zazunov, A. Brunetti, A. L. Yeyati, and R. Egger, *Phys. Rev. B* **90**, 104508 (2014).
- [10] See Supplemental Material at <http://link.aps.org/supplemental/10.1103/PhysRevLett.117.267701> for further details on the numerical and analytical methods used in this work, which includes Refs. [11,12].
- [11] A. Kamenev, *Field Theory of Non-Equilibrium Systems* (Cambridge University, Cambridge, England, 2011).
- [12] H. T. Chen, G. Cohen, A. J. Millis, and D. R. Reichman, *Phys. Rev. B* **93**, 174309 (2016).
- [13] L. S. Levitov, in *Quantum Noise in Mesoscopic Physics*, edited by Yu. V. Nazarov (Kluwer Academic, New York, 2002), p. 373.
- [14] W. Belzig and Yu. V. Nazarov, *Phys. Rev. Lett.* **87**, 197006 (2001).
- [15] A. Shelankov and J. Rammer, *Europhys. Lett.* **63**, 485 (2003).
- [16] A recent work points out the possibility of negative FCS arising in more general situations due to quantum interference; see P. P. Hofer and A. A. Clerk, *Phys. Rev. Lett.* **116**, 013603 (2016).
- [17] M. Esposito, U. Harbola, and S. Mukamel, *Rev. Mod. Phys.* **81**, 1665 (2009).
- [18] G. M. Tang, F. Xu, and J. Wang, *Phys. Rev. B* **89**, 205310 (2014).
- [19] R. Seoane Souto, R. Avriller, R. C. Monreal, A. Martín-Rodero, and A. Levy Yeyati, *Phys. Rev. B* **92**, 125435 (2015).
- [20] This corresponds to a relatively large broadening. As a reference, in Ref. [8], relaxation times of the order of 1–100 μ s have been reported, which would correspond to inelastic rates $1/\tau_{\text{in}} \sim 10^{-5}$ – 10^{-7} Δ in the case of Al.
- [21] A. Levy Yeyati, A. Martín-Rodero, and E. Vecino, *Phys. Rev. Lett.* **91**, 266802 (2003); A. Martín-Rodero and A. Levy Yeyati, *Adv. Phys.* **60**, 899 (2011).
- [22] We have further checked that the results are robust when the instantaneous switch on is replaced by a smooth one, provided that its rate is faster than the characteristic times for the ABS formation.
- [23] More strictly, Eq. (3) indicates an initial increase of $n_{\pm}(t)$ as t^2 for $t \lesssim 1/W$ followed by a linear increase for $1/W < t < 1/\Delta$.